International Journal of Optics and Applications 2015, 5(1): 10-21
DOI: 10.5923/j.optics.20150501.02

Effect of Polarization Controllers Rotation Angles on the Performance of Optically Generated UWB-Based Communication Systems

J. E. Kadum[1], R. S. Fyath[2,*]

[1]Department of Electronic and Communications Engineering, Al-Nahrain University, Baghdad, Iraq
[2]Department of Computer Engineering, Al-Nahrain University, Baghdad, Iraq

Abstract One of the interesting methods reported in the literature for photonic generation of impulse radio-ultrawideband (IR-UWB) signals is based on a phase modulator (PM) and an asymmetric Mach–Zehnder interferometer (AMZI). The AMZI is electrically reconfigurable by employing a polarization modulator (PolM). UWB signals with different modulation formats are realized by adjusting the polarization controllers (PC) in the AMZI and the amplitude of the electrical drive signal to the PolM. This paper addresses the effect of PCs rotation angles on the performance of on-off keying (OOK) and biphase modulation (BPM) systems based on Gaussian monocycle and doublet UWB pulses. The simulation results reveal that there are optimum values of these rotation angles that yield minimum bit-error-rate (BER) of the received UWB signals at the end of the transmission fiber link. Simulation results are presented using Optisystem Version 13.0.

Keywords Ultrawidwband-over-fibre, Photonic generation, Photonic microwave delay-line filter

1. Introduction

Ultrawideband (UWB) signals are applicable for short rang wireless communication systems, such as indoor wireless communication networks, intra-vehicle networks and wireless sensor network [1-4]. One of the versions of UWB-based communication is impulse radio (IR) which attracts increasing interest due to its intrinsic advantages, such as immunity to multipath fading, being carrier free, broad bandwidth, and low-power spectral density (PSD) [5-9]. The Federal Communication Commission (FCC) has allocated 7.5 GHz of spectrum for unlicensed use of UWB devices with 3.1-10.6 GHz band, with PSD less than -41.3 dBm/MHz for indoor wireless communication [10-12]. The UWB signals are characterized by a short propagation range which is generally limited, by the extremely low PSD, to a few meters to tens of meters [13]. To overcome the short propagation, UWB-over-fiber (UWBoF) systems have been proposed to increase the transmission range [14-16]. Thus, generation and distribution of UWB signals in the optical domain have attracted considerable interest. Several methods have been proposed in the literature for photonic generation of UWB signals. Some of these methods are based on nonlinear optical loop mirror [17, 18], Mach-Zehnder modulators [19, 20], polarization modulators [21-23], nonlinear fiber optics [24-26], optical filters [27, 28], phase modulation-to-intensity modulation conversion [29], or cascaded refractive semiconductor optical amplifiers [30]. One of the interesting methods for photonic generation of IR-UWB signals has been presented by Pan and Yao [31]. They have performed a comprehensive investigation technique to implement on-off keying (OOK), bi-phase modulation (BPM), pulse position modulation, pulse amplitude modulation, and pulse shape modulation. The method is based on phase modulator (PM) and an asymmetric Mach-Zehnder interferometer (AMZI) as shown in Fig. 1.

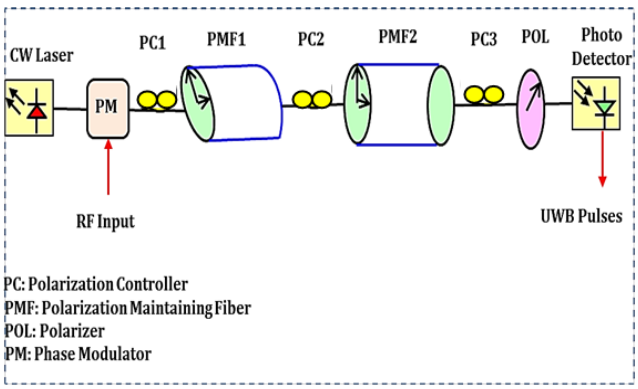

Figure 1. Schematic diagrams of the photonic microwave bandpass filter based on a phase modulator [31]

* Corresponding author:
rsfyath@yahoo.com (R. S. Fyath)
Published online at http://journal.sapub.org/optics
Copyright © 2015 Scientific & Academic Publishing. All Rights Reserved

The AMZI consists of two sections of polarization maintaining fiber (PMF) followed by a polarizer. Three polarization controllers (PCs) are inserted to adjust the polarization states of lightwaves before PMF1, PMF2, and the polarizer. The photodiode (PD) is connected at the output of the polarizer to perform optical to electrical conversion. The AMZI is electrically reconfigurable by employing a polarization modulator (PoLM). UWB signal with different modulation formats can be realized by adjusting these polarization controllers in the AMZI and the amplitude of the electric drive signal to the PolM. The study in [31] assumes fixed values for the rotation angles of the PCs ($\alpha_1 = 0$, 90° or 45°, $\alpha_2 = \alpha_3 = 45°$) in order to generate the various UWB modulation formats. To the authors' knowledge, the effect of deviations from these angle values is not addressed in the literature and this issue is investigated in this paper. The analysis presented in [31] is extended to take into account the effect of PC rotation angles. The simulation results reveal that there are optimum values of these angles that yield minimum bit-error-rate (BER) for the received UWB signals at the end of the transmission fiber. It is worth to mention here that this study can be considered as a first step toward analyzing optically generated UWB signals in the presence of components impairments and addressing its effect on the performance of UWBoF systems. This topic attracts little attention in the literature and the analysis and the results reported in this paper can be used as a guideline to investigate other optically generated UWB systems.

2. Analysis Framework

2.1. System Description

Figure 2 shows a simplified block diagram of the reconfigurable UWB system under investigation. The block diagram reflects the main components of the system in Fig. 1. To simplify the analysis, each PMF is modeled here by using three subcomponents. First, a polarization beam splitter (PBS) is used to resolve the incident field into two orthogonal polarization components. Then a time delay τ is introduced to one of the polarization components before combining them using a polarization beam combiner (PBC). The system of Fig. 2 consists of a laser diode (LD) operating in continuous wave (CW) mode, a phase modulator, an asymmetric Mach-Zehnder interferometer, and a photodiode.

The AMZI consists of two sections of PMFs followed by a polarizer. Three polarization controllers PC1, PC2 and PC3 are inserted to adjust the polarization of the optical wave before PMF1, PMF2 and the polarizer. Practically, the PD is the front-side of the optical receiver which receives the optical signal after transmission through an optical link. The effect of this link will be not taken into account in the analysis and its effect will be addressed through simulation. The input binary data d(t) is used to control a unipolar or bipolar switch driven by a series of a periodic short-duration Gaussian pulses to obtain OOK or BPM signaling, respectively. The gated Gaussian pulses are used to modulate the phase of CW laser through a PM which is modeled here using Mach-Zehnder modulator. The repetition rate of the Gaussian pulses is set equal to the bit rate of the binary data. Thus each of the data bit is spread by a single short Gaussian pulse. It is worth to mention here that this generating scheme is different from that adopted in [31] where the Gaussian pulses and the binary data are applied to the PM and PolM, respectively. Note further that the system in Fig. 2 does not use a PolM and hence can be used to generate OOK and BPM signaling only.

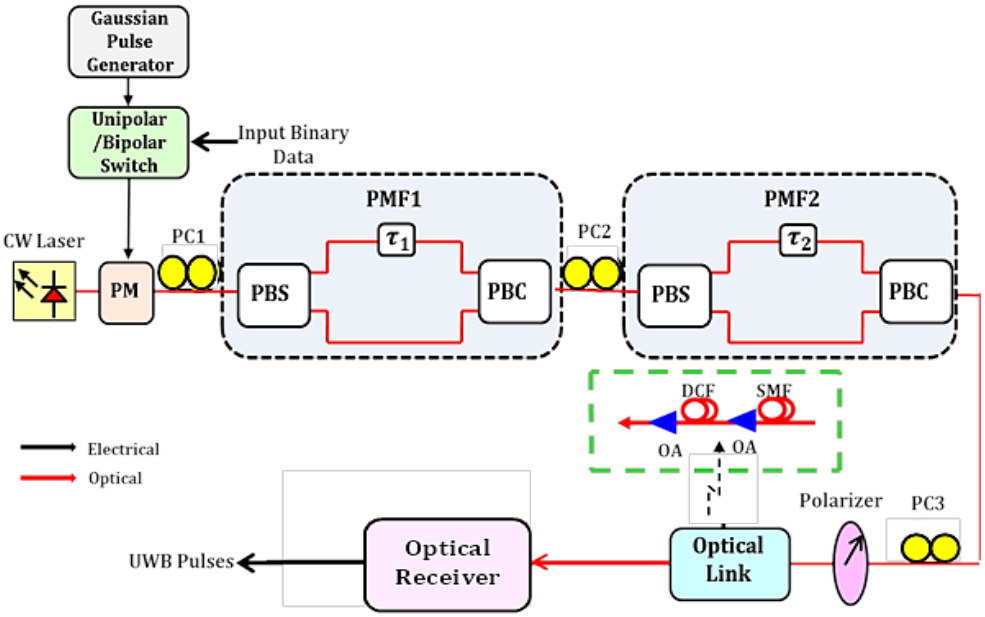

Figure 2. Configuration of the optical generation system. The insert shows the details of the transmission link

2.2. System Analysis

The normalized optical field at the output of the PM along the two polarization directions can be expressed as [31]

$$e_{PM}(t) = \begin{cases} \exp[j\omega_c t + jm\, d(t)g(t)] \\ 0 \end{cases} \quad (1)$$

where ω_c is the angular frequency of the optical carrier, m is the phase modulation index, $g(t)$ is a normalized Gaussian pulse, and d(t) is the input binary data. The binary data d(t) is given by

$$d(t) = \begin{cases} 1 \\ 0 \end{cases} \text{ OOK}$$

$$d(t) = \begin{cases} 1 \\ -1 \end{cases} \text{ BPM} \quad (2)$$

The complex transfer functions of PC and PMF can be expressed as

$$T_{PC}(\omega) = \begin{bmatrix} \cos\alpha\, e^{j\emptyset} & -\sin\alpha \\ \sin\alpha & \cos\alpha \end{bmatrix} \quad (3a)$$

$$T_{PMF}(\omega) = \begin{bmatrix} e^{j\omega\tau} & 0 \\ 0 & 1 \end{bmatrix} \quad (3b)$$

where α and $\emptyset$ are, respectively, the rotation angle and phase shift introduced by the PC while τ represents the time delay between the two polarization components introduced by the PMF. The complex transfer function of the cascaded optical components (three PCs and two PMFs) can be computed using the following relation

$$T(\omega) = T_{PC3}(\omega).T_{PMF2}(\omega).T_{PC2}(\omega).T_{PMF1}(\omega).T_{PC1}(\omega) \quad (4)$$

If the polarizer is adjusted to select the optical signal in the direction [1 0], the optical field at the output of the polarizer can be computed from

$$E_{POL}(\omega) = [1 \quad 0].T(\omega).E_{PM}(\omega) \quad (5)$$

where $E_{PM}(\omega)$ is the Fourier transform of the phase modulated signal and given by

$$E_{PM}(\omega) \equiv \mathcal{F}\{e_{PM}(t)\} = \begin{bmatrix} \mathcal{F}\{exp\left[j\omega_c t + jm_{eff}\, g(t)\right]\} \\ 0 \end{bmatrix} \quad (6)$$

where $\mathcal{F}\{.\}$ denotes the Fourier transform of the argument and m_{eff} represents the effective phase modulation index; $m_{eff} \equiv md(t)$ with d(t) takes the values 0, 1, or -1 according to the logic states and signaling format. Following the analysis reported in [31], the optical field at the polarizer output can be expressed in frequency and time domains as follows

$$E_{POL}(\omega) = \{\cos\alpha_1 \cos\alpha_2 \cos\alpha_3 \exp(j[\omega(\tau_1+\tau_2) + \emptyset_1 + \emptyset_2 + \emptyset_3]) - \cos\alpha_1 \sin\alpha_2 \sin\alpha_3 \exp(j[\omega\tau_1 + \emptyset_1]) - \cos\alpha_3 \sin\alpha_2 \sin\alpha_1 \exp(j[\omega\tau_2 + \emptyset_3]) - \cos\alpha_2 \sin\alpha_1 \sin\alpha_3\} \times \mathcal{F}\{[\exp(j\omega_c t + jm_{eff}\, g(t)] \quad (7)$$

$$e_{POL}(t) = \mathcal{F}^{-1}\{E_{POL}(\omega)\} = -\exp(j\omega_c t)\Big\{\cos\alpha_2 \sin\alpha_1 \sin\alpha_3 \exp\left(jm_{eff}\, g(t)\right) + \cos\alpha_1 \sin\alpha_2 \sin\alpha_3 \exp\big(j[\theta_1 + m_{eff}\, g(t+\tau_1)]\big) + \cos\alpha_3 \sin\alpha_2 \sin\alpha_1 \exp\big(j[\theta_3 + m_{eff}\, g(t+\tau_2)]\big) - \cos\alpha_2 \cos\alpha_1 \cos\alpha_3 \exp\big(j[\theta_1 + \theta_3 + \emptyset_2 + m_{eff}\, g(t+\tau_1+\tau_2)]\big)\Big\} \quad (8)$$

where $\mathcal{F}^{-1}\{.\}$ stands for the inverse Fourier transform, $\theta_1 = \omega_c\tau_1 + \emptyset_1$ and $\theta_3 = \omega_c\tau_2 + \emptyset_3$.

3. Generation of the UWB Signals

3.1. Gaussian Monocycle

To generate an UWB Gaussian monocycle, the polarization direction of the modulated light wave should be aligned with one principal axis of PMF1 (i.e., $\alpha_1 = 90^\circ$) and let $\theta_3 = 90^\circ$, $\emptyset_2 = 0$ [31]. Equation 8 is simplified to

$$e_{POL}(t) = -\exp(j\omega_c t)\{\cos\alpha_2 \sin\alpha_3 \exp\left(jm_{eff}\, g(t)\right) + \cos\alpha_3 \sin\alpha_2 \exp\left(j[\pi/2 + m_{eff}\, g(t+\tau_2)]\right)\} \quad (9)$$

Let $A = \cos\alpha_2 \sin\alpha_3$, $B = \cos\alpha_3 \sin\alpha_2$ and using the identities $\cos\left(x + \frac{\pi}{2}\right) = -\sin(x)$ and $\sin\left(x + \frac{\pi}{2}\right) = \cos(x)$ yields

$$e_{POL}(t) = -\exp\ (j\omega_c t)\{A[\cos\left(m_{eff}\, g(t)\right) + j\sin\left(m_{eff}\, g(t)\right) + B[-\sin\left(m_{eff}\, g(t+\tau_2)\right) + j\cos\left(m_{eff}\, g(t+\tau_2)\right)]\} \quad (10)$$

For a small-signal modulation, $|m_{eff}|$ is very small, $\sin(m_{eff}\, g(t)) \approx m_{eff}\, g(t)$ and $\cos\ (m_{eff}\, g(t)) \approx 1$, then

$$e_{POL}(t) = -\exp\ (j\omega_c t)\{\left[A - B\, m_{eff}\, g(t+\tau_2)\right] + j\left[A\, m_{eff}\, g(t) + B\right]\} \quad (11)$$

If the optical signal expressed in eqn. 11 is sent to a PD for square-law detection, the photocurrent is

$$i_{ph}(t) = |e_{POL}(t)|^2 = \left|-\exp\ (j\omega_c t)\{\left[A - B\, m_{eff}\, g(t-\tau_2)\right] + j\left[A\, m_{eff}\, g(t) + B\right]\}\right|^2$$

$$= A^2 - 2AB\ m_{eff}\, g(t+\tau_2) + B^2\left(m_{eff}\, g(t+\tau_2)\right)^2 + B^2 + 2AB\, m_{eff} g(t) + A^2(m_{eff} g(t))^2$$

$$i_{ph}(t) = [A^2 + B^2] + 2AB\, m_{eff}\, [g(t) - g(t+\tau_2) \quad (12)$$

Investigation eqn.12 reveals that the photocurrent corresponds to a first-order difference equation for the Gaussian pulse with a gain $G_{DE} = AB$ in addition to a DC term $I_{DC} = A^2 + B^2$. Note that both G_{DE} and I_{DC} depend on the PCs rotation angles α_2 and α_3

$$G_{DE} = \frac{1}{4}\sin(2\alpha_2)\sin(2\alpha_3) \quad (13a)$$

$$I_{DC} = (cos\alpha_2\, sin\alpha_3)^2 + (cos\alpha_3\, sin\alpha_2)^2 \quad (13b)$$

For the special case of $\alpha_2 = \alpha_3 = 45°$ which is adopted in [31], eqn. 12 reduces to that reported in [31].

3.2. Gaussian Doublet

To generate an UWB Gaussian doublet, the polarization direction of the modulated lightwave should be oriented to have $45°$ with principal axis of PMF1 (i.e., $\alpha_1 = 45°$) and let $\theta_1 = \theta_3 = 90°$, $\emptyset_2 = 0$ [31]. Equation 8 is simplified to

$$e_{POL}(t) = -1/\sqrt{2}\exp\ (j\omega_c t)\{\cos\alpha_2\, sin\alpha_3 \exp\left(j\, m_{eff}\, g(t)\right) + sin\alpha_2 sin\alpha_3 \exp\left(j\left[\frac{\pi}{2} + m_{eff}\, g(t+\tau_1)\right]\right) + \cos\alpha_3\, sin\alpha_2 \exp\ \left(j\left[\frac{\pi}{2} + m_{eff}\, g(t+\tau_2)\right]\right) - \cos\alpha_2\, cos\alpha_3\ \exp\ \left(j[\pi + m_{eff}\, g(t+\tau_1+\tau_2)]\right)\} \quad (14)$$

Let $X = \sin\alpha_2 \sin\alpha_3$ and $Y = \cos\alpha_2 \cos\alpha_3$, then using the two trigonometric identities adopted in section 3.1 yields

$$e_{POL}(t) = -\frac{1}{\sqrt{2}}\exp(j\omega_c t).\{A\left[\cos\left(m_{eff}\, g(t)\right) + j\sin\left(m_{eff}\, g(t)\right)\right] + X\left[-\sin\left(m_{eff}\, g(t+\tau_1)\right) + j\cos\left(m_{eff}\, g(t+\tau_1)\right)\right] + B\left[-\sin\left(m_{eff}\, g(t+\tau_2)\right) + j\cos\left(m_{eff}\, g(t+\tau_2)\right)\right] + Y\ \left[\cos\left((m_{eff}\, g(t+\tau_1+\tau_2)\right) + j\sin\left((m_{eff}\, g(t+\tau_1+\tau_2)\right)\right]\} \quad (15)$$

For a small-signal modulation, one can show that

$$e_{POL}(t) = -\frac{1}{\sqrt{2}}\exp(j\omega_c t).\{\left((A+Y) - m_{eff}\,[Xg(t+\tau_1) + Bg(t+\tau_2)]\right) + j\left(m_{eff}\,[Ag(t) + Yg(t+\tau_1+\tau_2)] + (X+B)\right)\} \quad (16)$$

The photocurrent generated from the field described in eqn. 16 is given by

$$i_{ph}(t) = \left|-\frac{1}{\sqrt{2}}\exp(j\omega_c t).\{\left((A+Y) - m_{eff}\,[Xg(t+\tau_1) + Bg(t+\tau_2)]\right) + j\left(m_{eff}\,[Ag(t) + Yg(t+\tau_1+\tau_2)] + (X+B)\right)\}\right|^2$$

$$= \left[(A+Y)^2 + (X+B)^2 + 2m_{eff}\{(X+B)[Ag(t) + Yg(t+\tau_1+\tau_2)] - (A+Y)[Xg(t+\tau_1) + Bg(t+\tau_2)]\}\right] \quad (17)$$

Equation 17 contains a DC term $[(A+Y)^2+(X+B)^2]$ in addition to an ac term that reflects the second-order difference components. For special case of $\alpha_2=\alpha_3=45°$ which is adopted in [31], $A=B=X=Y=\frac{1}{2}$. This yields an ac term that is proportional to $g(t)+g(t+\tau_1+\tau_2)-g(t+\tau_1)-g(t+\tau_2)$. This result is in accord with that in [31].

4. Simulation Results

This section presents simulation results describing signal generation and transmission performance for both Gaussian monocycle and doublet UWBoF systems. The results are reported for both OOK and BPM modulation formats with 625 Mb/s data rate and 1550 nm operating wavelength. Time delays of PMF1 and PMF2 (τ_1 and τ_2) are 20.1 and 40.1 ps, respectively. Other parameter values used in the simulation are as given in Table 1.

Two types of transmission links are considered in the simulation. The first link consists of a single-mode fiber (SMF). The second link consists of a SMF and dispersion compensating fiber (DCF) along with their optical amplifiers. In this link, the average losses and dispersion is zero. The parameter values of SMF and DCF are listed in Table 2. This section contains two parts; the first part considers the case of $\alpha_1=\alpha_3=45°$ while the second part addresses the effect of deviations of these angles from 45° on system performance.

Table 1. Parameter values used in the simulation

Parameter	Value
Bit rate	625 Mb/s
Wavelength	1550 nm
FWHM of the Gaussian pulses	85 ps
CW laser power	0 dBm
MZM extinction ration	20 dB
MZM insertion loss	5 dB
MZM bias voltage	2 V
Optical amplifier noise figure	4 dB
Optical bandpass filter order	5
Optical bandpass filter depth	100 dB
Electrical bandpass filter order	5
Electrical bandpass filter depth	100 dB
Photodiodes dark current	10 nA
Photodiodes responsivity	1 A/W
Photodiodes thermal noise	1×10^{-22} W/Hz
Electrical amplifier noise	-60 dBm

Table 2. Optical fiber parameter values used in the simulation

Parameter	Value	
	SMF	DCF
Attenuation, α	0.2 dB/km	0.5 dB/km
Group velocity dispersion, D	17 ps/(ns.nm)	-85 ps/(ns.nm)
Dispersion slop, S	0.075 ps/nm^2/km	-0.3 ps/nm^2/km
Differential group delay	0.2 ps/km	0.2 ps/km
Effective area, A_{eff}	80 µm^2	22 µm^2
Nonlinear refractive index, n_2	26×10^{-21} m^2/W	26×10^{-21} m^2/W

4.1. Case of $\alpha_1=\alpha_3=45°$

Figure 3 shows the generated Gaussian monocycle and doublet waveform along with the ideal waveforms which are included here for comparison purpose.

The FWHM of the Gaussian pulse which is used to obtain all the waveforms is 85 ps. Note that the time-domain representation highlights that the signals generated in this work are in good agreement with the ideal waveforms. Received PSDs are simulated when photonically generated pulses are adopted in back-to-back transmission. A bandpass filter (3.1-10.6 GHz) is inserted after the PD to reconfigure the PSD according to FCC limit. The results are presented in Fig. 4 for both OOK and BPM formats and show that the PSDs of the generated signals are within FCC mask.

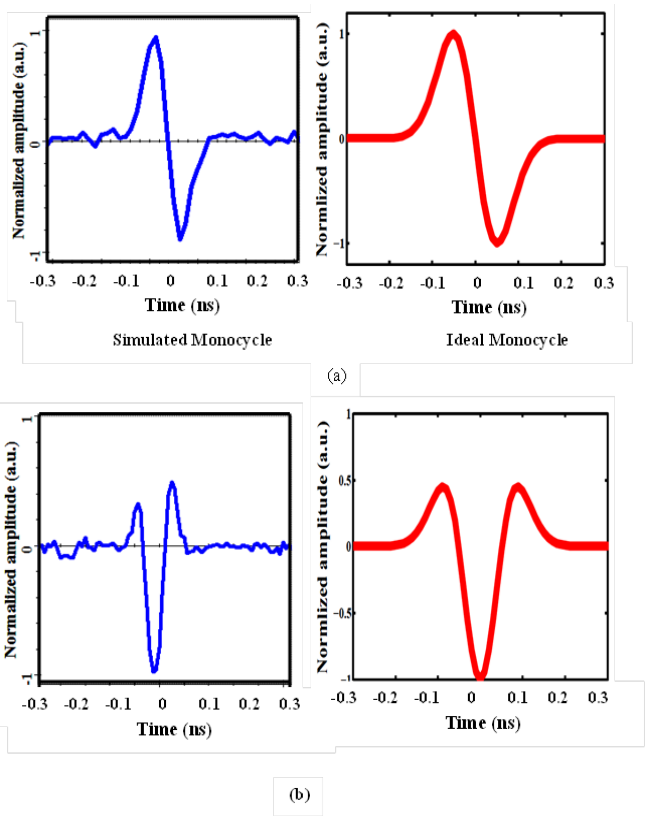

Figure 3. Simulated and ideal UWB pulses (a) Gaussian monocycle (b) doublet

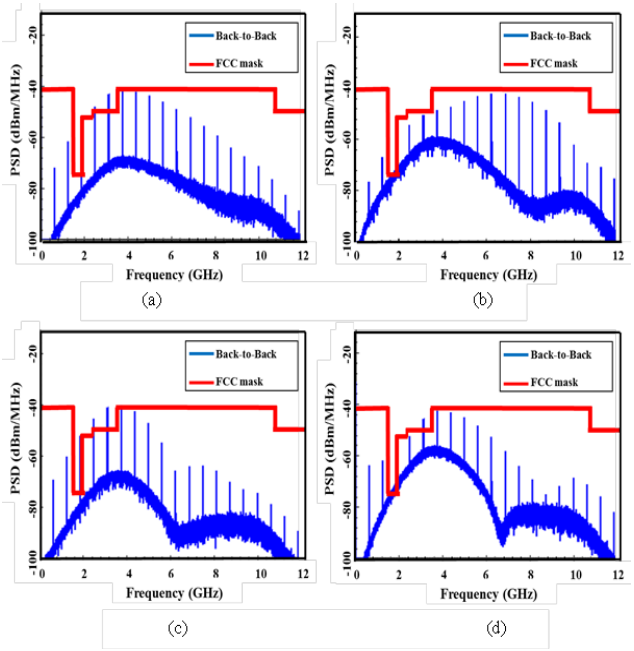

Figure 4. Power spectrum densities for back-to-back of (a) Gaussian monocycle OOK (b) Gaussian monocycle BPM (c) doublet OOK (d) doublet BPM

Figure 5 depicts the received eye diagrams when the generated signals are adopted in back-to-back transmission and used later to address the effect of fiber transmission link.

The simulation is carried further to address system performance when a SMF isused as the transmission link. No DCF or optical amplifiers are used to compensate the dispersion and losses of the fiber, respectively. Table 3 lists the lengths of the transmission fiber required to obtain a BER of $10^{-9}$for different signals and modulation formats. The corresponding received eye diagrams and PSDs are displayed in Figs. 6 and 7, respectively.

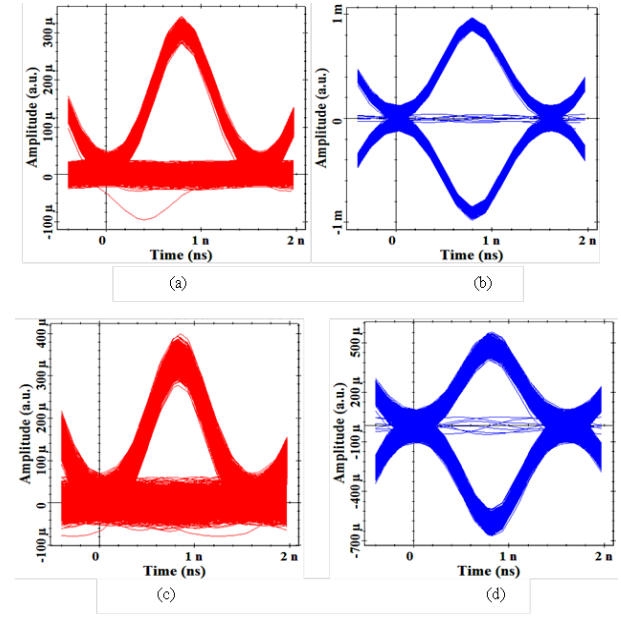

Figure 5. Eye diagrams of the received signals for back-to-back of (a) Gaussian monocycle OOK (b) Gaussian monocycle BPM (c) doublet OOK (d) doublet BPM

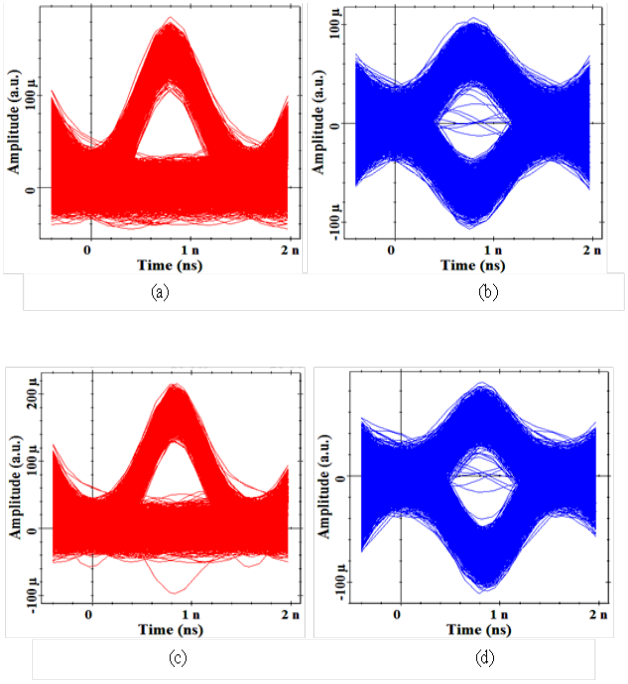

Figure 6. Eye diagrams of the received signals after transmission over SMF for (a) Gaussian monocycle OOK (b) Gaussian monocycle BPM (c) doublet OOK (d) doublet BPM

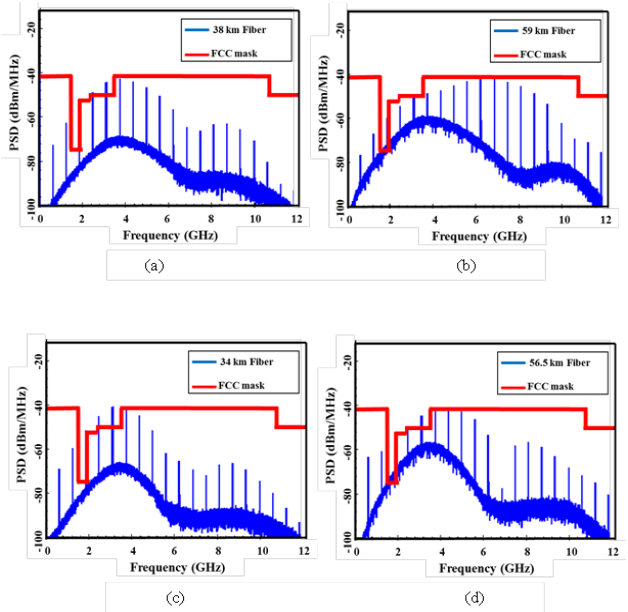

Figure 7. Power spectrum densities after transmission over SMF of (a) Gaussian monocycle OOK (b) Gaussian monocycle BPM (c) doublet OOK (d) doublet BPM

Table 3. SMF lengths at BER=10^{-9} for monocycle and doublet signaling systems operating with OOK and BPM modulation formats

Pulse Type	Modulation Format	SMF Length (km)
Gaussian Monocycle	OOK	38
	BPM	59
Doublet	OOK	34
	BPM	56.5

The next step is to investigate system performance when the transmission link consists of SMF and DCF along with their loss-compensation amplifiers. The results corresponding to a BER of 10^{-9} are listed in Table 4 and Figs. 8 and 9.

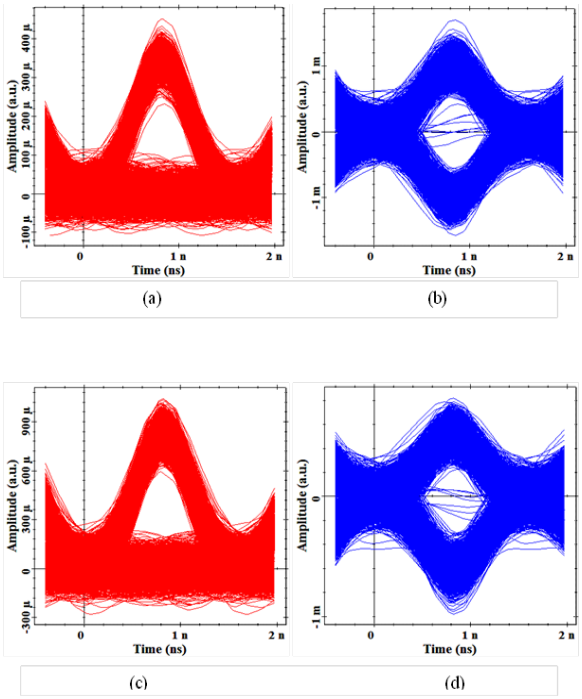

Figure 8. Eye diagrams of the received signals after transmission over optical link for (a) Gaussian monocycle OOK (b) Gaussian monocycle BPM (c) doublet OOK (d) doublet BPM

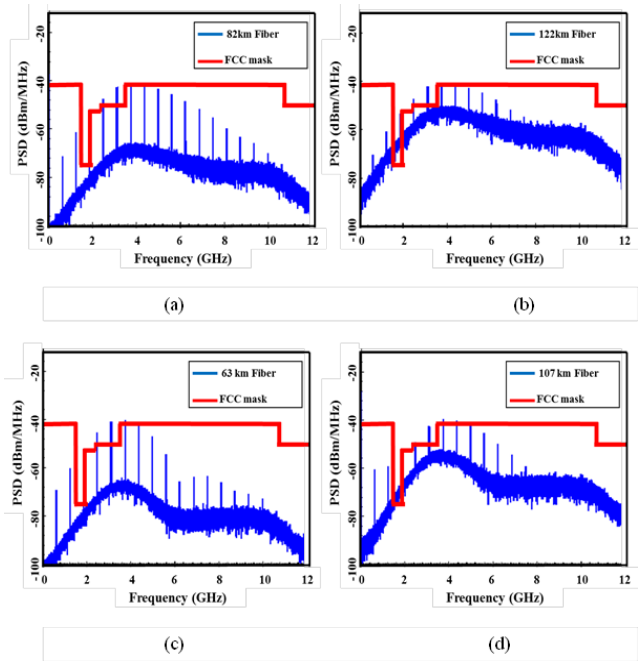

Figure 9. Power spectrum densities after transmission over optical link (SMF+DCF) for (a) Gaussian monocycle OOK (b) Gaussian monocycle BPM (c) doublet OOK (d) doublet BPM

Table 4. Transmission distances at BER=10^{-9} for monocycle and doublet signaling systems operating with OOK and BPM modulation formats

Pulse Type	Modulation Format	SMF Length (km)	Total Link Length (km)
Gaussian Monocycle	OOK	82	98.5
	BPM	122	146.5
Doublet	OOK	63	75.5
	BPM	107	128.5

Note that applying doublet signal reduces the total length of the transmission link to 0.77 and 0.87 of that of monocycle signaling for OOK and BPM, respectively.

4.2. Effect of Polarization Controllers Rotation Angles

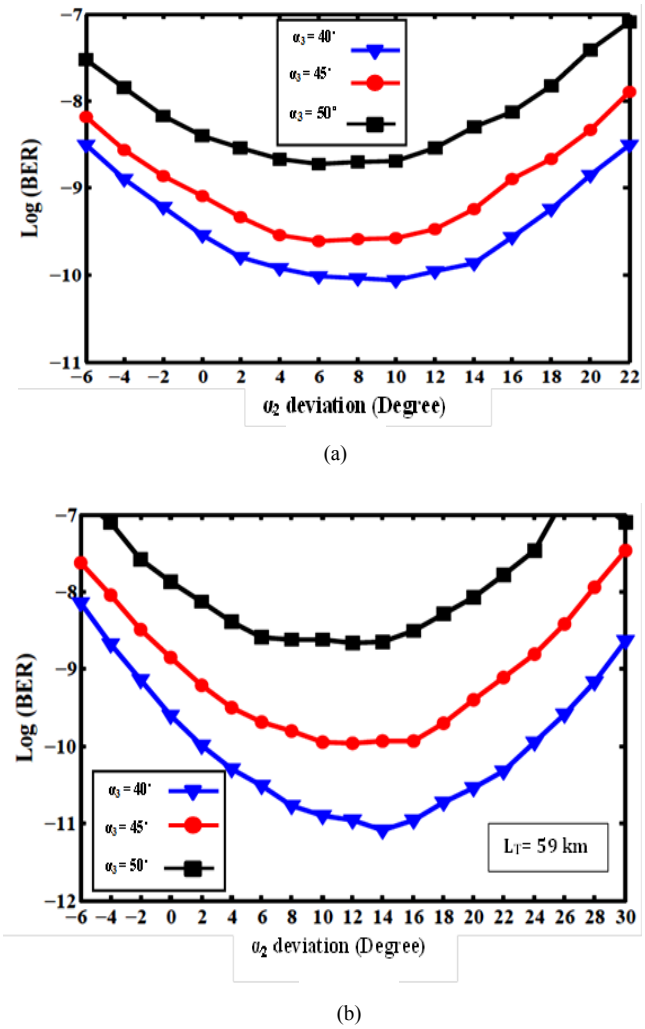

Figure 10. Variation of the BER with α_2 deviation for different values of α_3 after transmission over SMF for (a) Gaussian monocycle OOK (b) Gaussian monocycle BPM (c) doublet OOK (d) doublet BPM

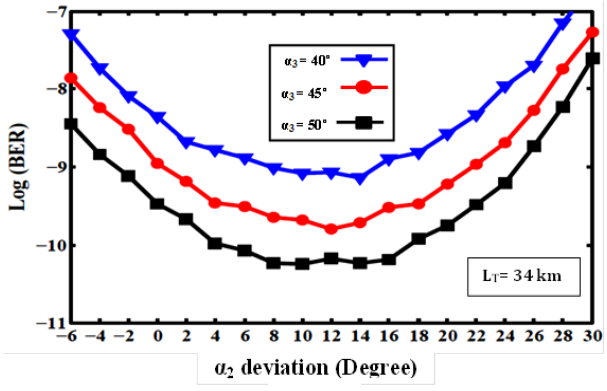

(c)

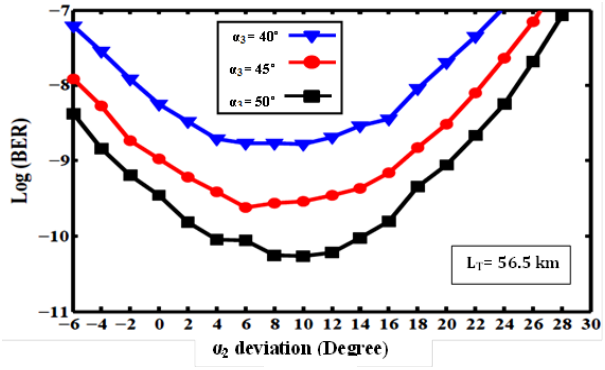

(d)

Figure 10. (Continued)

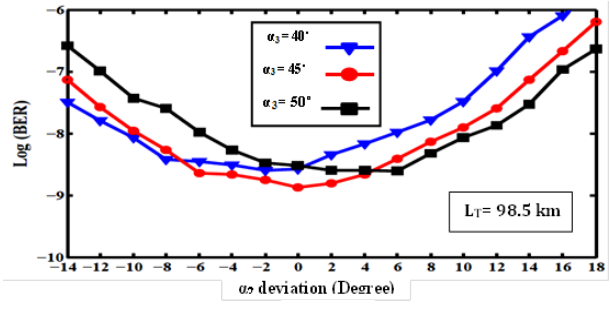

(a)

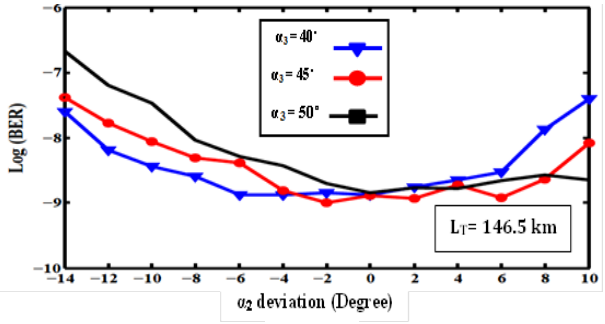

(b)

Figure 11. Variation of the BER with α_2 deviation for different values of α_3 after transmission over optical link (SMF+DCF) for (a) Gaussian monocycle OOK (b) Gaussian monocycle BPM (c) doublet OOK (d) doublet BPM

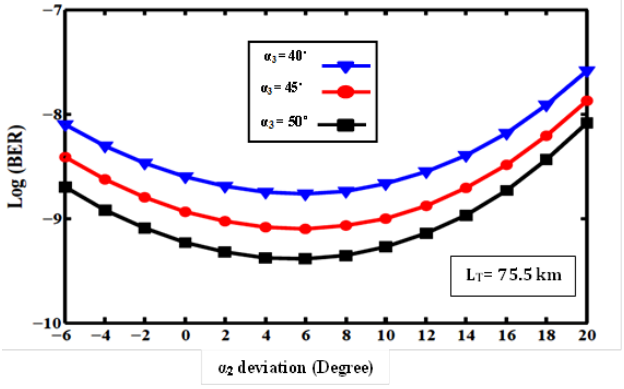

(c)

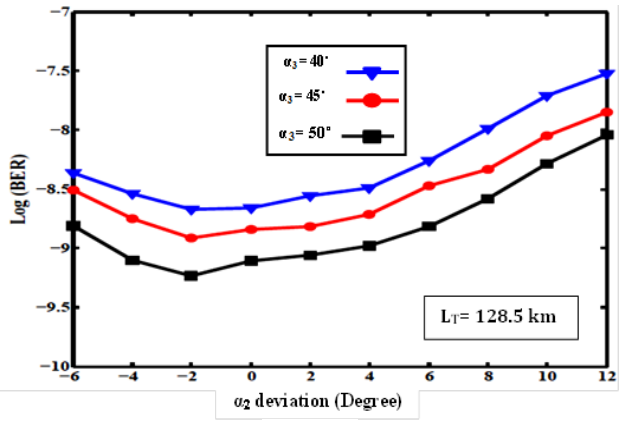

(d)

Figure 11. (Continued)

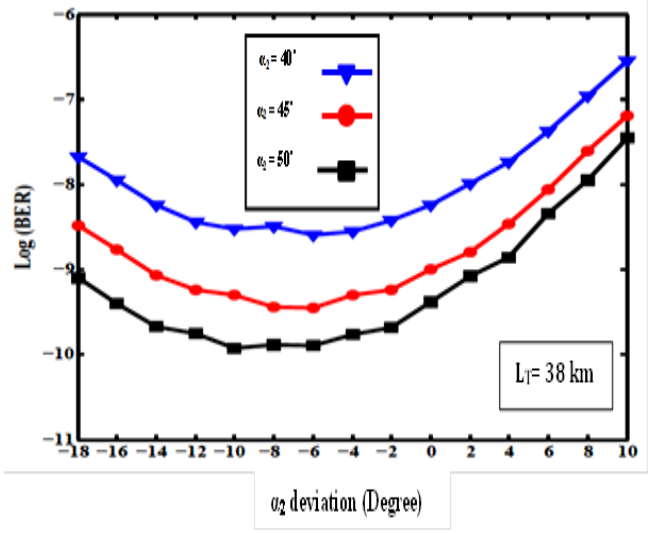

Figure 12. Variation of the BER with α_3 deviation for different values of α_2 for monocycle OOK signaling

Table 5. Optimum parameters of UWBoF systems using photonic generated Gaussian monocycle and doublet pulses

Link Type	Pulse Type	Modulation Format	Link Length (km)	Optimum Values			FoM
				Opt. α_2	Opt. α_3	Opt. BER	
Without Dispersion Compensation	Mono	OOK	38	56º	38º	9.2×10^{-11}	1.04
		BPM	59	58º	30º	3.0×10^{-13}	3.52
	Doublet	OOK	34	56º	58º	8.3×10^{-12}	2.08
		BPM	56.5	54º	58º	1.6×10^{-11}	1.80
With Dispersion Compensation	Mono	OOK	98.5	48º	48º	8.3×10^{-10}	0.08
		BPM	146.5	44º	46º	9.2×10^{-10}	0.04
	Doublet	OOK	75.5	50º	58º	1.8×10^{-10}	0.74
		BPM	128.5	44º	58º	1.7×10^{-10}	0.77

This subsection addresses the effect of deviations of the angles α_2 and α_3 on system performance. The results are presented for four systems, monocycle- and doublet-based OOK and BPM systems. The length of the transmission link is set equal to the length that yields a BER of 10^{-9} for each of the four systems. It is worth to mention here that the total photocurrent is applied to decision circuit to estimate the BER characteristics. This is in contrast to the technique adopted in [31] which uses only the ac components of the photocurrent to estimate system BER. The receiver adopted here uses DC coupled front-end amplifiers to maintain the DC component of the photocurrent. Figure 10 shows the variation of the BER with α_2 deviation and taking α_3 as independent parameter for the four systems under investigation. The transmission link is assumed to be consisted of a SMF only. Results related to a transmission link consisting of SMF, DCF and optical amplifiers are given in Fig. 11.

The results in Figs. 10 and 11 reveal that the BER performance can be improved by deviating $\boldsymbol{\alpha_2}$ from $\mathbf{45°}$ and this deviation depends on the value of $\boldsymbol{\alpha_3}$. This conclusion is also drawn when one consider the deviation of BER with $\boldsymbol{\alpha_3}$ for different values of $\boldsymbol{\alpha_2}$ (see Fig. 12 for monocycle OOK system).

The above results lead to the main finding that angles $\boldsymbol{\alpha_2}$ and $\boldsymbol{\alpha_3}$ should be chosen carefully to minimize the BER for each of the four systems. This is a two-dimensional optimization problem and it is here performed for the four systems and for both types of the transmission links. Table 5 lists the optimum values of $\boldsymbol{\alpha_2}$ and $\boldsymbol{\alpha_3}$ that give minimum BER. These results correspond to two transmission links, one consists of SMF while the other consists SMF and DCF with their optical amplifiers. The last column of this table lists the values of a performance measure parameter which is denoted by Figure of Merit (FoM)

$$\text{FoM} = \text{Log}\ \frac{\text{BER}\,(45^{\circ},45^{\circ})}{\text{BER}\,(\alpha_2,\alpha_3)} \qquad (18)$$

This parameter is introduced here to quantively measure the effect of deviations of rotation angles from 45° on system performance. The results in Table 5 indicate clearly that BER performance can be enhanced by optimizing the rotation angles $\boldsymbol{\alpha_2}$ and $\boldsymbol{\alpha_3}$ and this effect is more pronounced when the transmission link consists of a SMF only. The monocycle BPM system offers the best performance (FoM=3.52) when operates under optimum conditions. In contrast, the optimum rotation angles do not yield notable BER performance enhancement when the monocycle OOK and BPM system redesigned with fully loss and dispersion compensation.

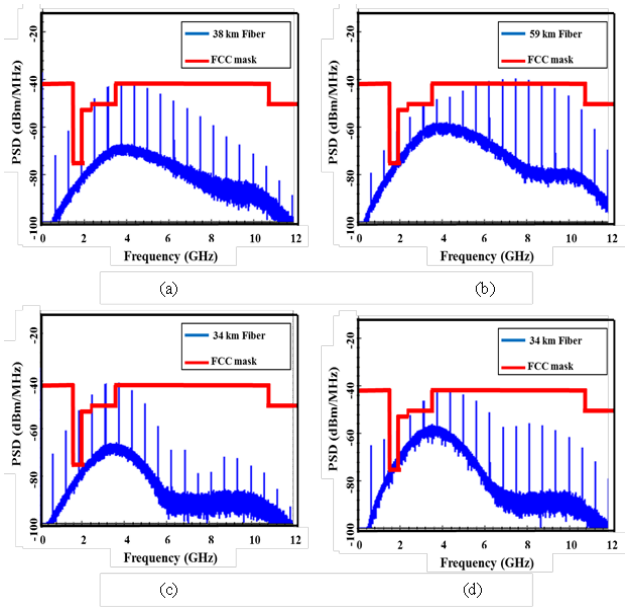

Figure 13. Optimum power spectrum densities after transmission over SMF of (a) Gaussian monocycle OOK (b) Gaussian monocycle BPM (c) doublet OOK (d) doublet BPM

The corresponding optimum PSDs and optimum received eye diagrams are given in Figs. 13-16.

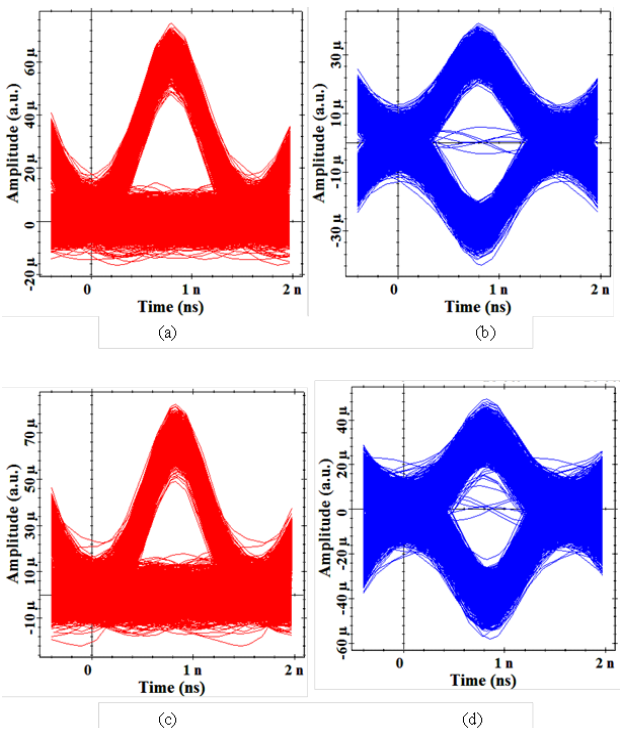

Figure 14. Optimum received eye diagrams after transmission over SMF of (a) Gaussian monocycle OOK (b) Gaussian monocycle BPM (c) doublet OOK (d) doublet BPM

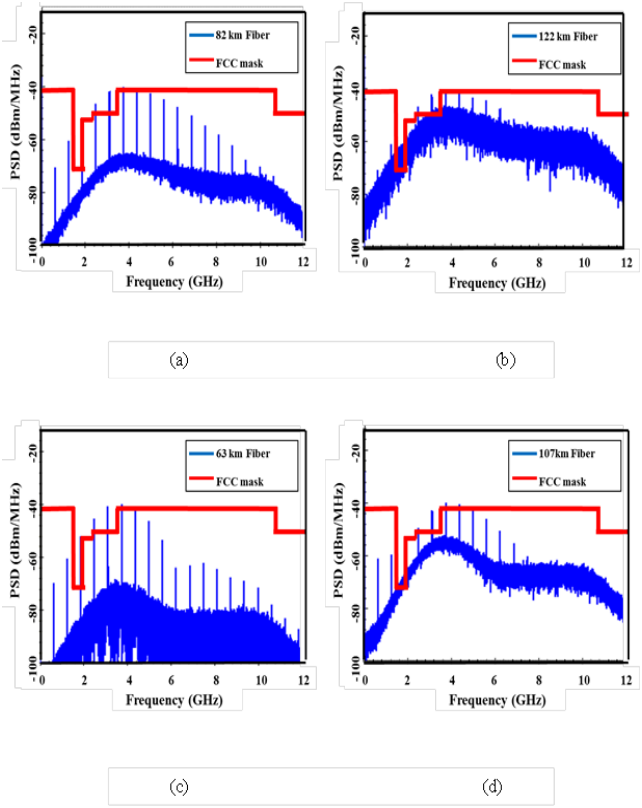

Figure 15. Optimum power spectrum densities after transmission over optical link (SMF+DCF) for (a) Gaussian monocycle OOK (b) Gaussian monocycle BPM (c) doublet OOK (d) doublet BPM

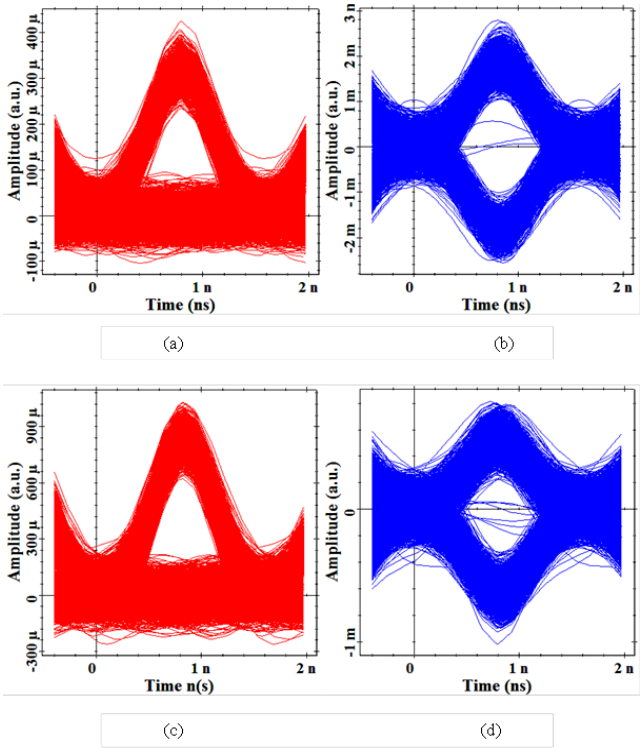

Figure 16. Optimum received eye diagrams after transmission over optical kink (SMF+DCF) for (a) Gaussian monocycle OOK (b) Gaussian monocycle BPM (c) doublet OOK (d) doublet BPM

5. Conclusions

The analysis presented in [31] has been extended to take into account the effect of PCs rotation angles on the transmission performance of optically generated Gaussian monocycle and doublet UWB pulses. Simulation results have been reported for 625 Mb/s fiber communication systems operating with or without dispersion compensating fiber. The simulation results reveal that the BER performance can be enhanced by optimizing the rotation angles of the polarization controllers and this effect is more pronounced when the transmission link consists of a SMF only. The monocycle BPM system offers the best performance (FoM=3.52) when operates under optimum conditions. In contrast, the optimum rotation angles do not yield notable BER performance enhancement when the monocycle OOK and BPM systems are redesigned with fully loss and dispersion compensation.

REFERENCES

[1] J. Wang, and J. Sun, "All-optical ultrawideband monocycle generation using quadratic nonlinear interaction seeded by dark pulses," IEEE Photonics Technology Letters, Vol. 22, No. 3, PP. 140-142, FEBRUARY, 2010.

[2] V. Moreno, M. Rius, J. Mora, M. A. Muriel, and J. Capmany, "UWB monocycle generator based on the non-linear effects of an SOA-integrated structure," IEEE Photonics Technology Letters, Vol. 26, No. 7, PP. 690-693, April, 2014.

[3] H. Feng, M. P. Fok, S. Xiao, J. Ge, Q. Zhou, M. Locke, R. Toole, and W. Hu, "A Reconfigurable high-order UWB signal generation scheme using RSOA-MZI structure," IEEE Photonics Journal, Vol. 6, No. 2, PP. 7900307-7900307, April, 2014.

[4] S. Pan, and J. Yao, "IR-UWB-over-fiber systems compatible with WDM-PON networks," Journal of Lightwave Technology, Vol. 29, No. 20, PP. 3025-3034, October, 2011.

[5] Y. Yu, J. Dong, X. Li, and X. Zhang," UWB monocycle generation and bi-phase modulation based on Mach–Zehnder modulator and semiconductor optical amplifier," IEEE Photonics Journal, Vol. 4, No. 2, PP. 327-338, April, 2012.

[6] P. Li, H. Chen, X. Wang, H. Yu, M. Chen, and S. Xie, "Photonic generation and transmission of 2-Gbit/s power-efficient IR-UWB signals employing an electro-optic phase modulator," IEEE Photonics Technology Letters, Vol. 25, No. 2, PP. 144-146, January, 2013.

[7] F. Zhang, S. Fu, J. Wu, N. Q. Ngo, K. Xu, Y. Li, X. Hong, P. Shum, and J. Lin, "UWB impulse radio transmitter using an electrooptic phase modulator together with a delay interferometer," IEEE Photonics Technology Letters, Vol. 22, No. 20, PP. 1479-1481, October,2010.

[8] X. Yu, T. B. Gibbon, R. Rodes, T. T. Pham, and I. T. Monroy, "System wide implementation of photonically generated impulse radio ultra-wideband for gigabit fiber-wireless access," Journal of Lightwave Technology, Vol. 31, No. 2, PP. 264-275, January, 2013.

[9] M. Beltrán, and R. Llorente, "Dual photonic generation ultrawideband impulse radio by frequency shifting in remote-connectivity fiber," Journal of Lightwave Technology, Vol. 29, No. 24, PP. 3645-3653, December,2011.

[10] P. Li, H. Chen, M. Chen, and S. Xie, "Gigabit/s photonic generation, modulation, and transmission for a reconfigurable impulse radio UWB over fiber system," IEEE Photonics Journal, Vol. 4, No. 3, PP. 805-816, June, 2012.

[11] M. Mirshafiei, A. Ghazisaeidi, D. Lemus, S. LaRochelle, and L. A. Rusch, "Upconversion of gain-switched laser pulses for optical generation of UWB signals," Journal of Lightwave Technology, Vol. 30, No. 2, PP. 207-214, January, 2012.

[12] Z. Hu, J. Sun, J. Shao, and X. Zhang, "Filter-free optically switchable and tunable ultrawideband monocycle generation based on wavelength conversion and fiber dispersion," IEEE Photonics Technology Letters, Vol. 22, No. 1, PP. 42-44, January, 2010.

[13] V. Moreno, M. Rius, J. Mora, M. A. Muriel, and J. Capmany, "UWB doublet generation employing cross-phase modulation in a semiconductor optical amplifier mach–zehnder interferometer," IEEE Photonics Journal, Vol. 5, No. 6, PP. 7101106- 7101106, December, 2013.

[14] W. Li, L. X. Wang, J. Y. Zheng, M. Li, and N. H. Zhu, "Photonic generation of ultrawideband signals with large carrier frequency tunability based on an optical carrier phase-shifting method," IEEE Photonics Journal, Vol. 5, No. 6, PP. 5502007-5502007, October, 2013.

[15] M. Abtahi, and L. A. Rusch, "RoF delivery over PONs of optically shaped UWB signals for Gigabit/s wireless distribution in the home," IEEE Journal On Selected Areas In Communications, Vol. 29, No. 6, PP. 1304-1310, June, 2011.

[16] Y. M. Chang, J. Lee, D. Koh, H. Chung, and J. H. Lee, "Ultrawideband doublet pulse generation based on a semiconductor electroabsorption modulator and Its distribution over a fiber/wireless link," Journal Of Optical Communications Networks, Vol. 2, No. 8, PP. 600-608, August, 2010.

[17] T. Huang, J. Li, J. Sun, and L. R. Chen, "Photonic generation of UWB pulses using a nonlinear optical loop mirror and Its distribution over a fiber link," IEEE Photonics Technology Letters, Vol. 23, No. 17, PP. 1255-1257, September, 2011.

[18] B. Luo, J. Dong, Y. Yu, and X. Zhang, "Bandwidth-tunable single-carrier UWB monocycle generation using a nonlinear optical loop mirror," IEEE Photonics Technology Letters, Vol. 24, No. 18, PP. 1646-1649, September, 2012.

[19] Y. Yu, J. Dong, X. Li, and X. Zhang, "Ultra-wideband generation based on cascaded Mach–Zehnder modulators," IEEE Photonics Technology Letters, Vol. 23, No. 23, PP. 1754-1756, December, 2012.

[20] P. Cao, X. Hu, J. Wu, L. Zhang, X. Jiang, and Y. Su, "Reconfigurable UWB pulse generation based on a dual-drive Mach–Zehnder modulator," IEEE Photonics Journal, Vol. 6, No. 5, PP. 7903206- 7903206, October,2014.

[21] W. Zhihu, W. Rong, P. Tao, S. Guodan, F. Tao, "Switchable optical ultra-wideband pulse generator based on polarization modulator," China Communications, PP. 113-117, July, 2013.

[22] Y. M. Chang, J. Lee, H. S Lee, L. Yan, and J. H. Lee, "Generation and distribution of 1.25 Gb/s Ultrawideband doublet pulses based on the combination of nonlinear polarization rotation and parametric amplification," Journal Of Lightwave Technology, Vol. 29, No. 6, PP. 931-938, March, 2011.

[23] Y. Min Chang, J. Lee, and J. H. Lee, "Bismuth nonlinear optical fiber for photonic ultrawideband radio-signal processing," IEEE Journal Of Selected Topics In Quantum Electronics, Vol. 18, No. 2, PP. 891-898, April, 2012.

[24] Y. Peled, M. Tur, and A. Zadok, "Generation and detection of ultra-wideband waveforms using stimulated brillouin scattering amplified spontaneous emission," IEEE Photonics Technology Letters, Vol. 22, No. 22, PP. 1692-1694, November, 2010.

[25] E. Zhou, X. Xu, K. S. Lui, and K. K. Y. Wong, "Photonic ultrawideband pulse generation with HNL-DSF-based phase and intensity modulator, " IEEE Photonics Technology Letters, Vol. 23, No. 7, PP. 396-398, April, 2011.

[26] A. Zadok, Xi. Wu, J. Sendowski, A. Yariv, and A. E. Willner, "Photonic generation of ultra-wideband signals via pulse compression in a highly nonlinear fiber," IEEE Photonics Technology Letters, Vol. 22, No. 4, PP. 239-241, February, 2010.

[27] J. Zheng, N. Zhu, L. Wang, J. Liu, and H. Liang, "Photonic generation of ultrawideband (UWB) pulse with tunable notch-band behavior," Vol. 4, No. 3, PP. 657-662, June, 2012.

[28] C. Yang, L. Xia, S. Fu, and D. Liu, "Reconfigurable UWB

pulse generation based on multi-taps and a programmable filter," IEEE Photonics Technology Letters, Vol. 26, No. 14, PP. 1395-1398, July, 2014.

[29] E. Zhou, X. Xu, K. S. Lui, and K. K. Y. Wong, "A power-efficient ultra-wideband pulse generator based on multiple PM-IM conversions," IEEE Photonics Technology Letters, Vol. 22, No. 14, PP. 1063-1065, July, 2010.

[30] H. Feng, S. Xiao, L. Yi, and W. Hu, "Photonic generation of reconfigurable orders ultrawideband signals by using cascaded RSOAs," IEEE Photonics Technology Letters, Vol. 26, No. 9, PP. 908-910, May, 2014.

[31] S. Pan, and J. Yao, "UWB-over-fiber communications: modulation and transmission," Journal of Lightwave Technology, Vol. 28, No. 16, PP. 2445-2455, August, 2010.